Recent improvements of the stromal topography system and new in vitro results (12th of Dec 2000)

1 System improvements

During the past few weeks most of the data was gathered using a shadow projection principle for imaging the fringe pattern on the cornea. We placed the absorption grating some 60mm away from the cornea into the collimated beam. Parts of the beam were absorbed by the grating leaving a shadow on the cornea. This shadow of the grating already allowed very precise measurements as confirmed on calibrating samples.

We now even further improved on the accuracy by using a self designed imaging lens system which is derived from a 193nm lithography 4 lens system. It magnifies the grating by a factor of four and has a small numerical aperture and thus a large focussing depth. The working distance is about 500mm.

In the following graph identical measurements on a flat surface of a plane/concave lens with the old and the new system are compared:

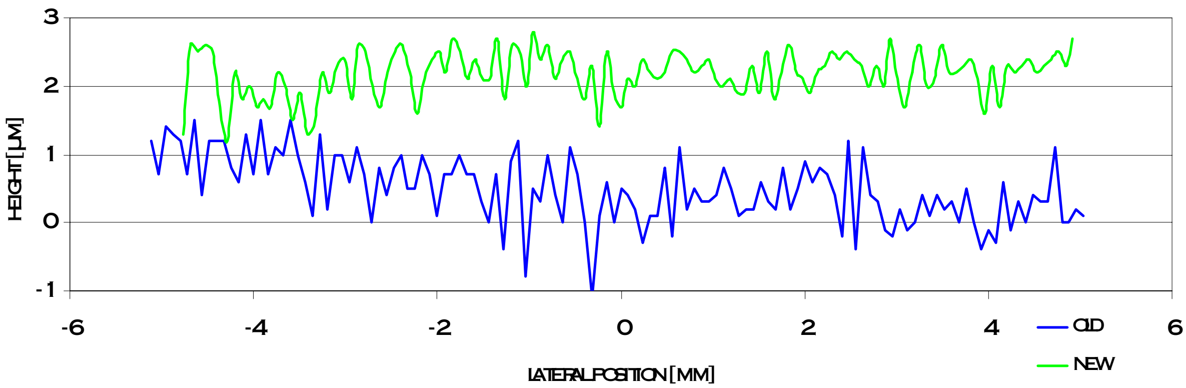

While the blue curve represents an accuracy within ± 1 micron achieved with the shadow projection, the green line has about ± 0.5 microns. The improved accuracy can be attributed to the sharper projection which increases the contrast of the lines and thus enhances the output of the evaluation algorithm. This improvement also has an influence on the quality of the stromal fluorescence images and thus on the measurement accuracy on corneas.

2 Automatic treatment modus

Our new demonstration system consists of a flying spot laser which incorporates the real time measurement device. It currently allows treatments in 1 diopter steps with intermediate measurements. The final diopter is ablated according to the preceding steps. The actual ablation rate is measured during these first steps. It is then applied to the final step which also does the fine tuning. The following figures display elevation maps of such a 4 diopter treatment. The color scales cover 30 microns in the 1 diopter maps and 60 microns in the 1-3 diopter and the full treatment maps. The difference maps always cover 40 microns. The white areas in the difference maps indicate a deviation of the performed from the intended ablation of less than +/-2.5 microns.

1st diopter:

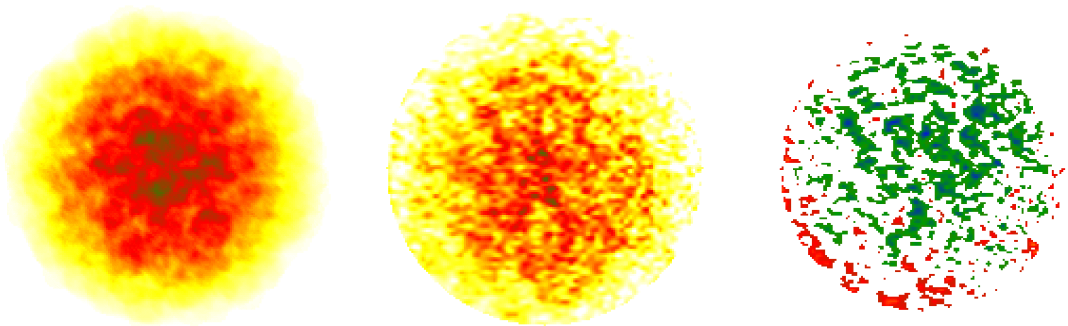

Intended ablation performed ablation difference

A slight undercorrection appears in the upper right corner.

2nd diopter:

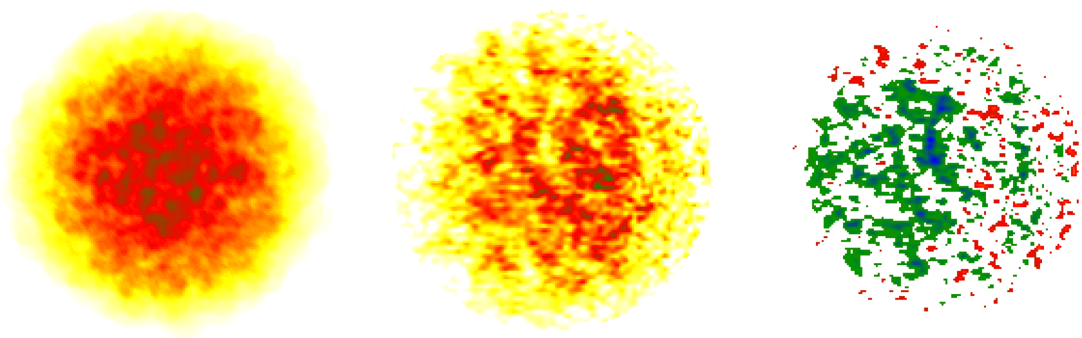

Intended ablation performed ablation difference

The left part seems undercorrected here.

3rd diopter:

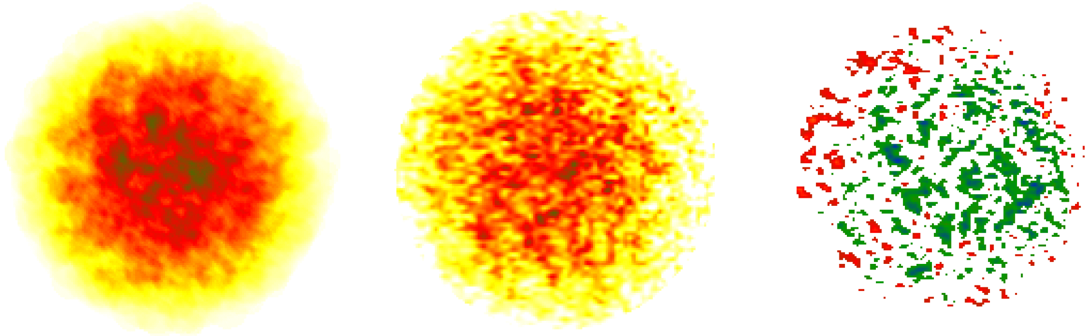

Intended ablation performed ablation difference

Here the right region is undercorrected. All of these first three treatments were slightly undercorrected. This leads to a considerable undercorrection in the sum of the three which is shown in the following figures.

1st three diopters:

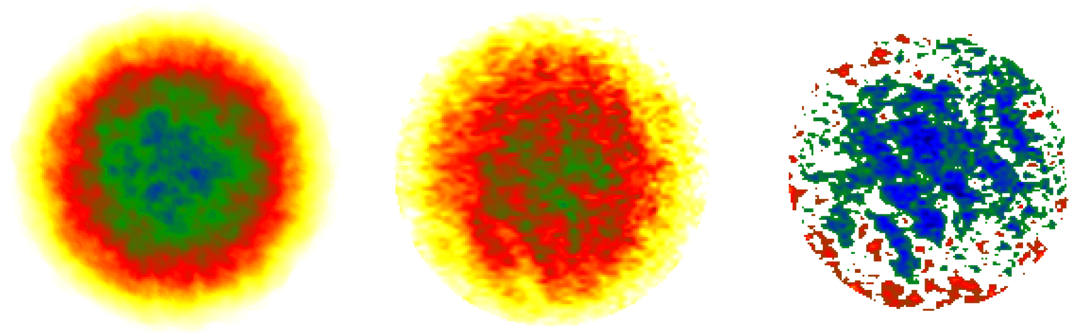

Intended ablation performed ablation difference

The difference map clearly reveals an increased deviation of the performed ablation from the intended. The errors induced during each of the three steps increase sum up to a large total. This total error is removed in the final step. Here are the corresponding maps:

Final individual correction:

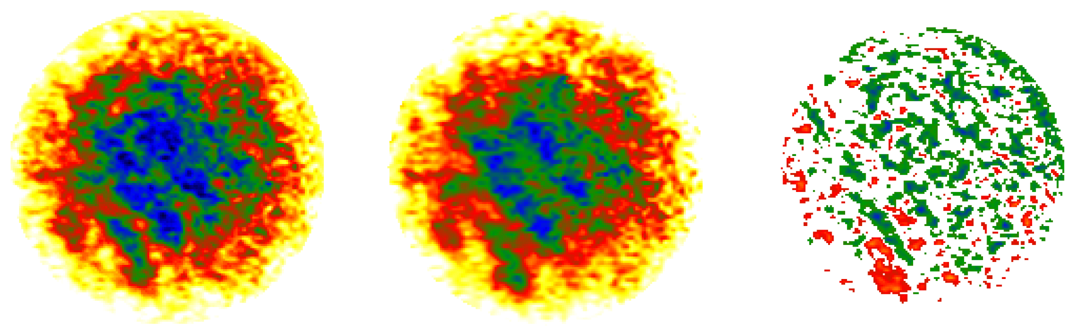

Intended ablation performed ablation difference

The irregular intended ablation pattern is required due to the errors of the first three steps. The difference map shows that this pattern was ablated with a better homogeny than each of the preceding steps. The reason is that the treatment was individually guided according to measurements performed beforehand. This was not the case for the first three steps. The accuracy of the whole treatment is thus only depending on the last step's accuracy. This is shown in the comparison of the whole treatment maps.

Whole 4 diopter treatment:

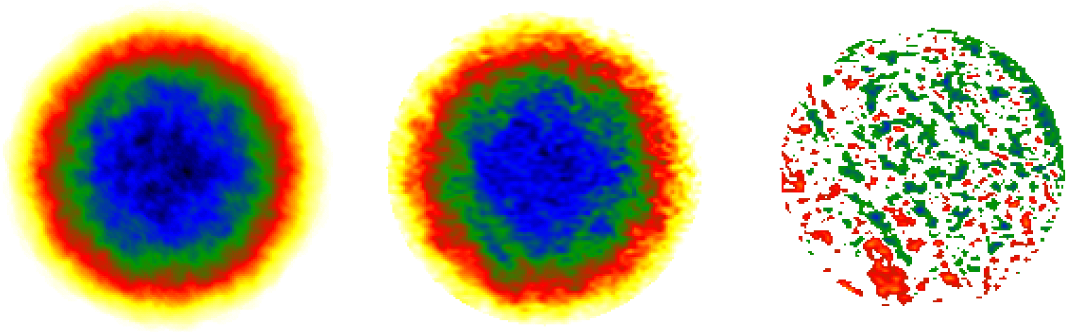

Intended ablation performed ablation difference

The difference map of the whole intended and measured treatment is similar to the final correction difference map as all errors induced by the first steps were corrected in this final step. Thus only the final step deviations remain.

These experiments have shown that an individual correction of errors induced during a standard treatment is feasible using the online measurement device. A real guidance of the laser pulses is performed with an individually calculated ablation pattern. This ensures a much lower deviation of the final surface from the intended map than achievable without stromal topography guided fine tuning.

3 New in vitro experiments

3.1 Biomechanics

With this improved system we performed some new tests that one cannot do on patients. These tests might further the understanding of the ongoing processes during and after the treatments of patients.

Freshly excised procine corneae were treated in a PTK mode with our flying spot system. Air was blown into the anterior chamber to prevent aqueous humor from entering the corneal tissue. The intraocular pressure was set to 20mmHg. The diameter of the treatment zone was 4mm, its depth was approximately 60 microns. The following figures show the treatment in two different high scales.

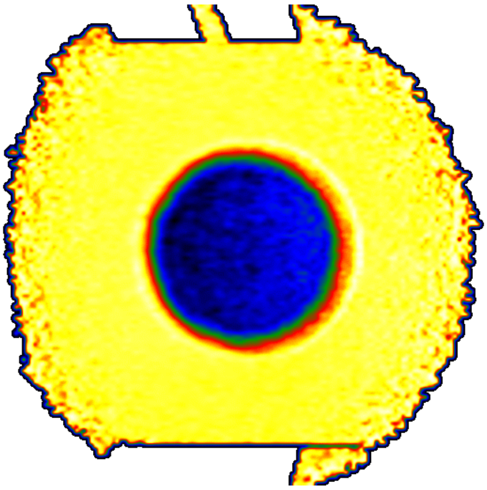

PTK treatment: 70 microns scale

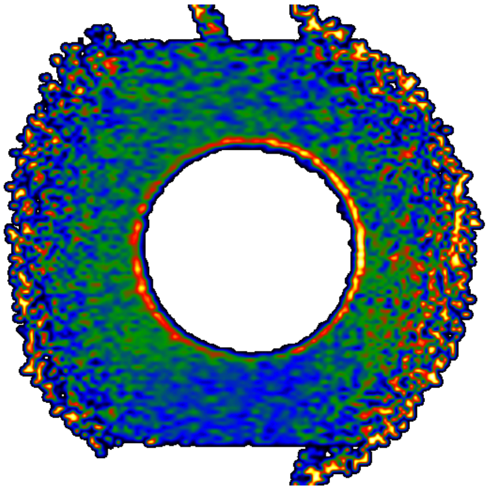

PTK treatment: 15 microns scale

The left figure shows the whole treatment. The colors in the right figure are selected to match the untreated region of the cornea to reveal changes due to biomechanical reactions of the tissue. At the edge of the treatment zone the tissue is raised along a thin ring. Further outside there is no significant effect visible directly after the treatment.

The following image is a different example of a very steep 250 microns deep laser cut into the cornea and its influence on the surrounding tissue surface. There is a very strong reaction leading to a height change of more than 50 microns compared to the periphery that extends more than 2 mm laterally. This example is far from being representative for refractive laser surgery. It rather resembles RK cuts.

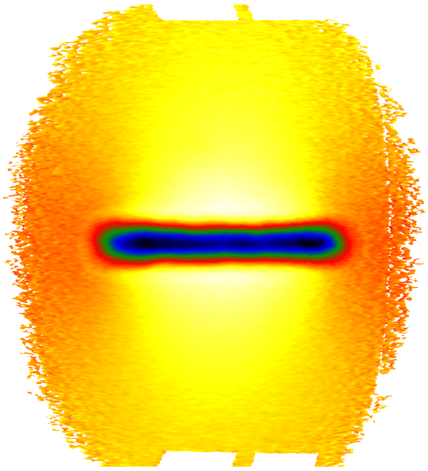

The findings of the first images are confirmed in the following horizontal line scans:

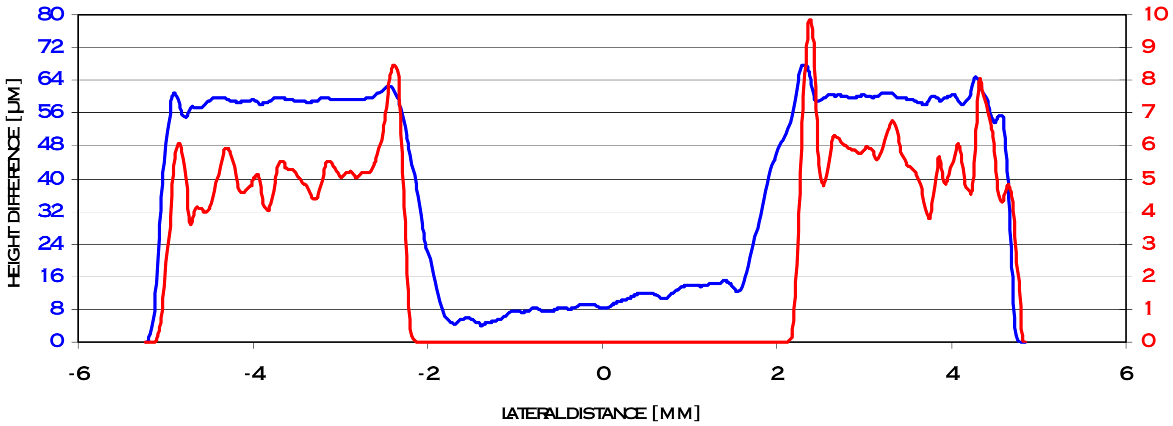

The blue line's scale is on the left of the graph, the red line's scale is on the right. The surface roughness as measured is smaller than 3 microns, the height of the ring was measured to be between 3 and 5 microns immediately after the treatment.

We did these measurements on several samples in preparation of an ARVO abstract. We found a strong correlation between the slope of the treatment crater edge and the height of the tissue ring extending above the cornea. In very steep craters the height reached values up to 50 microns as shown above. Here is a graph that summarizes the findings:

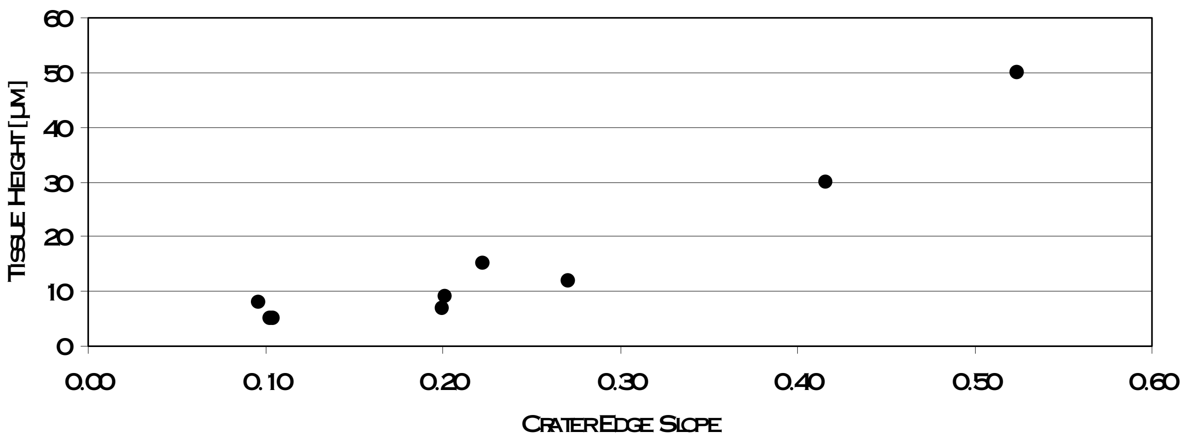

The increasing tissue height might be correlated with biomechanical reactions of the lamellae in the cornea. We assume that they rearrange depending on the tissue cutting angle (or slope). As soon as there is sufficient adhesion between the cut lamella and its adjacent lower lamella the increase in height at the cutting edge is fairly small.

3.2 Temporal development

We were also interested in the development of the treated surface as time goes on. In regular time steps of up to 20 minutes measurements were taken to assess this development.

Here are four images at 1, 5, 10 and 20 minutes for which the shape directly after the treatment served as a reference:

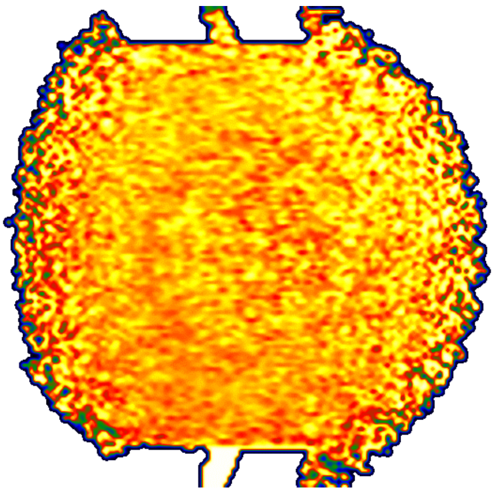

Height difference 1 min post PTK

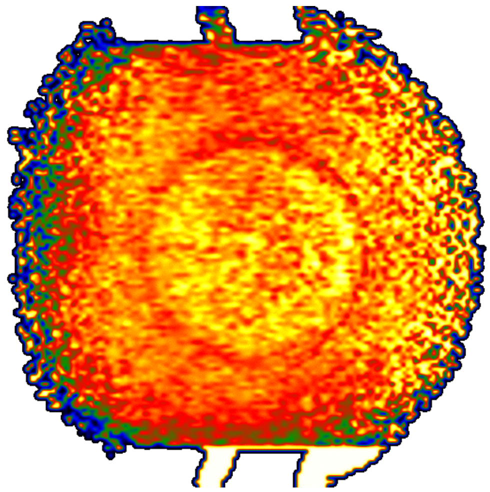

Height difference 5 min post PTK

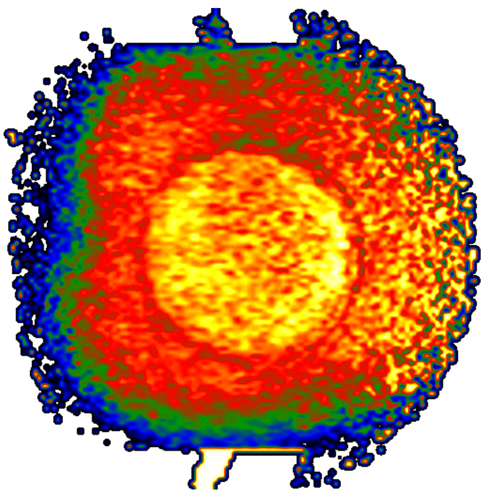

Height difference 10 min post PTK

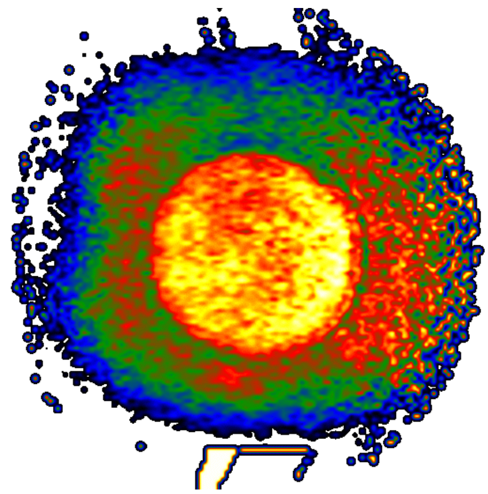

Height difference 20 min post PTK

The height scale in these images is 20 microns for the color coded 256 grey values. The images show a pretty stable central region that corresponds with the 4 mm treatment zone. In contrast the periphery constantly decreases in height with time. These findings are confirmed in the horizontal line scans through the images.

This first graph shows the height difference of the surfaces after the given time intervals.

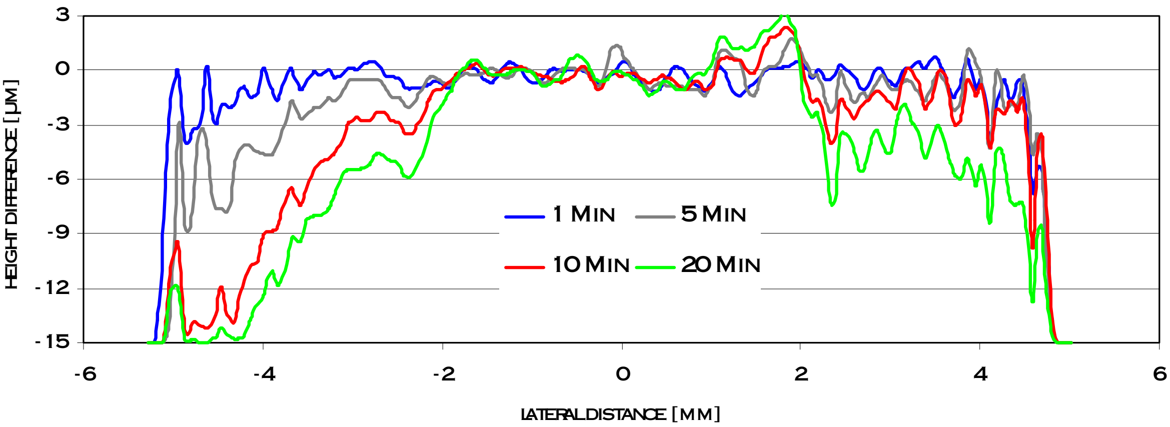

The structure of the lines stays similar for each measurement time. This allows the conclusion that the details of the surface are measured within the claimed accuracy. On the other hand there is a decrease in height with time that might be attributed to the loss of water and a subsequent shrinking. Surprisingly this effect does not occur in the treated area. One might assume that this surface is either sealed by the treatment such that further evaporation of water is impossible. Or there is a constant delivery of water into this region from the inner parts of the corneal lamellae that are cut within the treatment zone. Or this region is already completely dry after the treatment.

The following graph shows the height change rate of the surface depending on the distance from the treatment zone:

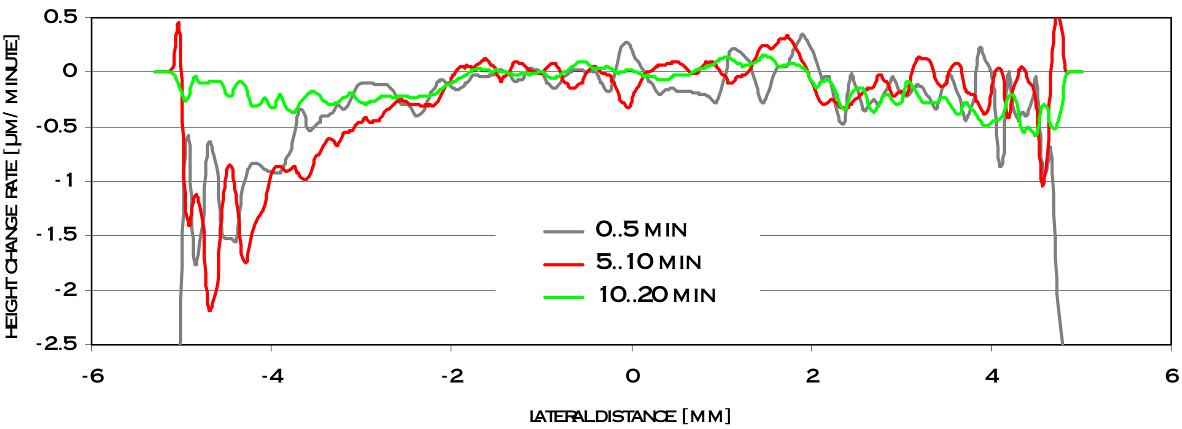

There is hardly any difference between the rate within the first and the second 5 minutes after the end of the treatment. During the time frame of 10 to 20 minutes the rate decreased considerably to less than 0.5 microns per minute. Probably there was no water left to evaporate at that time. Further studies of this kind will be performed in the future to improve the statistics of these findings.

3.3 Flap thickness measurements

During our patient measurements we already gained some preliminary information on the flap geometry. There was some evidence that the central part of the flap is much thinner than the outer regions. This might explain cases of buttonholes.

To further study these phenomena we measured cuts on porcine eyes. An ACS (B&L) was used with 130 and 160 micron plates. We measured before and after cutting. Alignment of the measurements was done by minimizing tilt in the difference maps. Here are some examples:

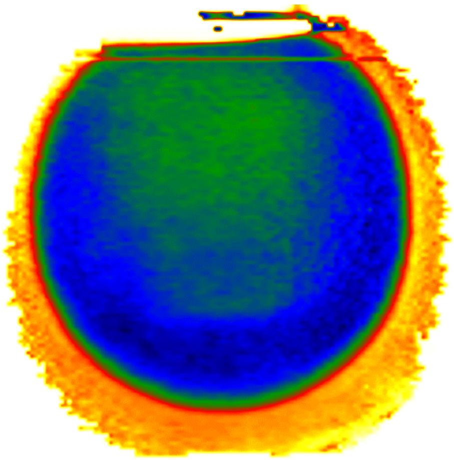

Flap 1: 160μm plate, 260μm color scale

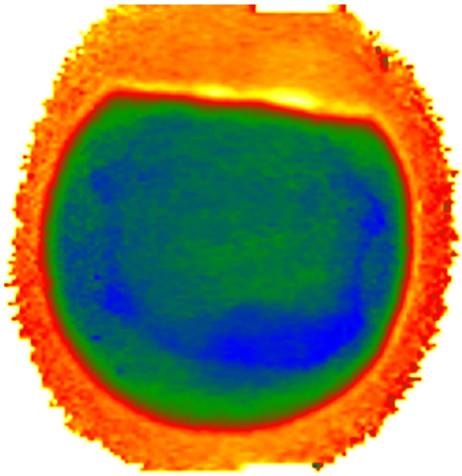

Flap 2: 130μm plate, 180μm color scale

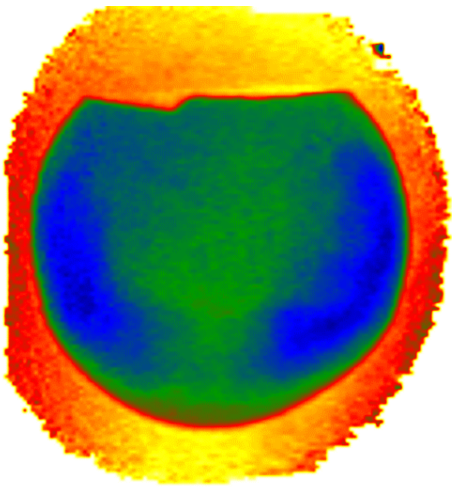

Flap 3: 130μm plate, 180μm color scale

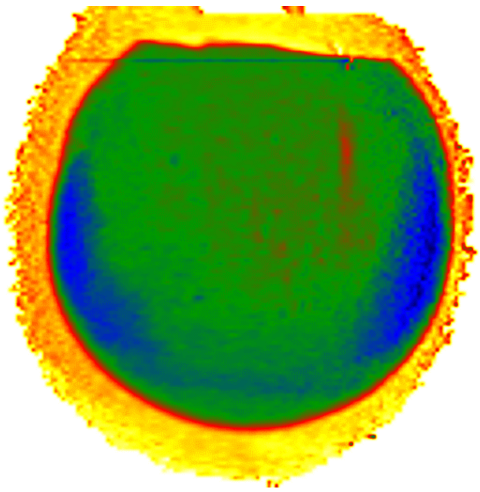

Flap 4: 130μm plate, 200μm color scale

All flaps show a decreased central thickness extending along the cutting direction. This finding is corresponding well with the measurements done on patients during the clinical trials with different other microkeratoms. The following graph gives an idea of the absolute thickness values and the shape of the flap. It is a horizontal cut through flap 3.

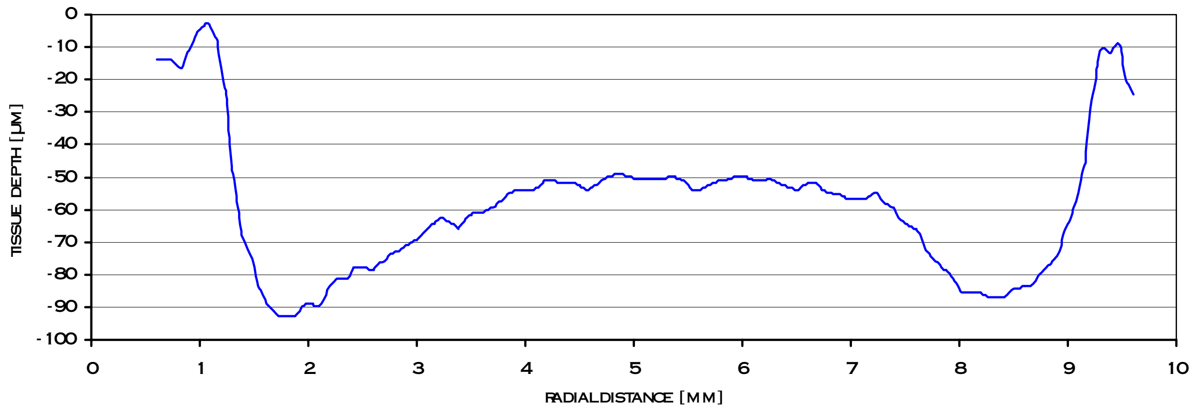

The graph indicates a maximum cutting depth of approximately 90 microns with a central flap thickness of only 50 microns. A 130 micron plate was used in this case.